



Lacustrine record of centennial- and millennial-scale rainfall variability of the East Asian summer monsoon during the last deglaciation: Multi-proxy evidence from Taiwan

Xiaodong Ding^a, Liwei Zheng^a, Dawei Li^a, Tien-Nan Yang^b, Teh-Quei Lee^b, Shuh-Ji Kao^{a,*}

^a State Key Laboratory of Marine Environmental Science, Xiamen University, Xiamen 361102, China

^b Institute of Earth Sciences, Academia Sinica, Taipei 115, Taiwan

ARTICLE INFO

Article history:

Received 3 September 2015

Received in revised form 24 January 2016

Accepted 22 February 2016

Available online 2 March 2016

Keywords:

High resolution

East Asian summer monsoon

Last deglaciation

Southern Taiwan

ABSTRACT

Situated at the border between the Southeast Asian continent and the northwestern Pacific, Taiwan's climate is primarily influenced by the East Asian Summer Monsoon (EASM) and episodic tropical cyclones formed in the western Pacific. The lake sediments in Taiwan thus potentially archive the information of typhoon events and past monsoon variability. A high-resolution multi-proxy (total carbon, mass accumulation rate of total carbon, weight percent of wood fragments, $\delta^{13}\text{C}$ of the organic carbon, magnetic susceptibility, chemical weathering index) and well-dated lacustrine record from Dongyuan Lake ($22^{\circ}10'N$, $120^{\circ}50'E$; 360 m above sea level) in southern Taiwan was used to reconstruct centennial to millennial timescale EASM oscillations specifically for the transition from the last deglaciation to the Early Holocene (17–9 ka BP). The temporal patterns of proxies on both timescales in our records broadly agree with those in the Greenland ice core, which shows enhanced EASM during the warm period and weakened monsoon during the cold period. Different from northern high-latitude climates, we found two phases in the Mystery Interval, opposite Bølling–Allerød (BA) trend with maximum monsoonal rainfall in the Allerød period and more gradual transition to Younger Dryas event in our record. Likely, other climate forcings beyond the North Atlantic climate jointly modulated the EASM. Changes of sea surface temperature in the western tropical Pacific also might have exerted synergistic control on EASM precipitation in Taiwan on the centennial timescale during the last deglaciation. In addition, several high sedimentation events accompanied by significant amounts of wood fragments were observed and coincide with the paleo-record of mass wasting events identified on various downstream floodplains in Taiwan. Since mass wasting processes were rainfall-driven and threshold-triggered, such coherence possibly indicated an intensification of typhoon activity during the early Holocene. More high-resolution lacustrine records are required to decipher the hydrological variation and climate dynamics that were co-influenced by the Intertropical Convergence Zone (ITCZ) and typhoon activity in Southeast Asia.

© 2016 Elsevier B.V. All rights reserved.

1. Introduction

The East Asian Monsoon (EAM) is an important component of the global climate system and plays a significant role in global hydrologic and energy cycles. The evolution of the EAM is a principal and direct factor that has influenced the past environment in East Asia, particularly the amount and distribution of precipitation on both local and regional scales that directly determines the prosperity of livelihood of tens of thousands of people who live in monsoonal regions in East Asia (An, 2000). A full understanding of the EAM variability in the past and its forcing mechanisms is vital to accurately predict its future evolution.

The history of the EAM has been explored since the early 1990s (An, 2000 and references therein). The precise timing and structure of

East Asian Summer Monsoon (EASM) variability in different timescales have been well established by Chinese stalagmite records over the past decade (Cai et al., 2006; Cheng et al., 2006, 2009, 2012; Dykoski et al., 2005; Liu et al., 2008, 2013; Ma et al., 2012; Wang et al., 2001, 2005, 2008; Yang et al., 2010; Yuan et al., 2004). The East Asian monsoon is characterized by orbitally controlled cycles, punctuated by millennial and sub-millennial timescale events and synchronous with northern high latitude climate variation (e.g., Cheng et al., 2006; Liu et al., 2013; Ma et al., 2012; Wang et al., 2001, 2008). The climate variability during the last deglaciation (Termination I) is one of the most intriguing areas of paleoclimate research due to a serial abrupt climatic fluctuations including millennial scale events such as the “Mystery Interval” (MI, 17.5–14.5 ka BP, Denton et al., 2006), Bølling–Allerød Interstadial (BA, 14.5–12.9 ka BP) and Younger Dryas Stadial (12.9–11.7 ka BP) and sub-millennial scale events (i.e., Older Dryas, OD; Intra-Allerød Cold Period, IACP), which may advance our understanding of earlier abrupt

* Corresponding author.

E-mail address: sjkao@xmu.edu.cn (S.-J. Kao).

climate change (Genty et al., 2006) and help us to assess future environmental changes under modern global warming. The consistency in the timing and duration of the millennial and sub-millennial scale events during the last deglaciation as observed in Chinese Speleothem records and Greenland temperature records provides evidence for a teleconnection between the EASM system and the climate in northern high latitudes (Dykoski et al., 2005; Ma et al., 2012; Wang et al., 2001; Wang et al., 2005; Yang et al., 2010).

However, the climatic interpretation, particularly the moisture sources, of stalagmite records still remains debatable (Maher and Thompson, 2012; Pausata et al., 2011). Recently, the variation of $\delta^{18}\text{O}$ in Chinese stalagmite records was proposed to reflect “a mean state of summer monsoon intensity or integrated moisture transport rather than local precipitation” (Cheng et al., 2012). A recent model study further corroborated this view (Liu et al., 2014). Although the authors suggested that the stalagmite $\delta^{18}\text{O}$ records in China do represent the intensity of EASM, these records do not seem to be related to the rainfall changes in southeastern China (Liu et al., 2014). Nevertheless, high-resolution and well-dated records of the EASM prior to the Holocene are almost exclusively from Chinese stalagmite studies. In addition, the correlation between EASM precipitation and the sea surface temperature in the tropical Pacific in the past remains ambiguous, although several reports have suggested the variation of sea surface temperature (SST) in the western tropical Pacific also might have important impacts on the EASM (Cai et al., 2010; Selvaraj et al., 2007, 2011; Zhong et al., 2015). Thus, more independent high-resolution natural archives, especially for the low latitude regions, are urgently needed to fully understand the EASM variability, particularly the magnitude, frequency and forcing mechanisms of the EASM during the last deglaciation.

Taiwan Island is located off the southeastern coast of mainland China and sits along the front edge of the East Asian monsoon range; therefore, it is geographically suitable for exploring past monsoon variability through its natural archives such as lake sediment and peat deposits (Lee et al., 2010, 2014; Li et al., 2013; Liew et al., 2006a, 2006b, 2014; Selvaraj et al., 2007, 2011, 2012; Wang et al., 2014, 2015; Yang et al., 2011, 2014). The climate of Taiwan is mainly influenced by the East Asian monsoon system superimposed by episodic tropical cyclones (typhoons). On average, 3–4 typhoons make landfall during late summer and early fall every year (Chen and Chen, 2003). The total rainfall of Taiwan is very high (3300 mm) and tropical cyclones account for as high as 47.5% of the total (Chen et al., 2010). In addition to typhoon rain, a strong seasonality can be observed with warm and wet seasons during the boreal summer (May–September) and relatively cool and dry seasons during the winter (October–April). Because of typhoon-induced high precipitation (and thus high erosion and sedimentation rates) and strong tectonic activities, Taiwan Island has the world's largest physical weathering rate (Kao and Milliman, 2008; Li, 1976); therefore, the lacustrine sediment records in Taiwan are generally younger than the last glacial period except for a few longer records (e.g., Liew et al., 2006a; Yang et al., 2011). The ~14.5-m-long core TYP-B retrieved from Dongyuan Lake in southern Taiwan fortunately covered the last 21 ka. Previously, palynological records and sedimentary organic matter have been published in low temporal resolution to infer vegetation change and monsoonal rainfall evolution (Lee and Liew, 2010; Yang et al., 2011). Due to their relatively lower sampling resolution, the fine structures and mechanisms of the climate oscillation variability during the last deglaciation and Early Holocene have not been revealed and discussed. In this study, we present a multi-proxy record (total carbon, mass accumulation rate of total carbon, weight percent of wood fragments, $\delta^{13}\text{C}$ of the organic carbon, magnetic susceptibility and chemical weathering index) with high sampling resolution for the period of the last deglaciation from Dongyuan Lake in southern Taiwan. The fine structures of climate oscillation variability are thus reconstructed, which facilitates a comparison with other records from mainland China and the North Atlantic region to examine different climatic responses at centennial to millennial scale.

2. Geographical setting and modern climate

Dongyuan Lake (22°10'N, 120°50'E; 360 m above sea level), is located along the northern edge of a hilly basin in southern Taiwan, near the head waters of Mudan River (Fig. 1). At present, the lake has a surface area of $2 \times 10^4 \text{ m}^2$. The lake level is less than 2 m and the drainage area covers approximately $94 \times 10^4 \text{ m}^2$ and ranges from 360 m to 500 m a.s.l. The surrounding catchment of Dongyuan Lake is covered by lowland subtropical evergreen forest (Lee and Liew, 2010). According to instrumental records from a nearby meteorological station, the contemporary average monthly air temperatures in the study area vary between 20.7 °C and 28.4 °C with an annual mean temperature of 25.1 °C (Fig. 1C). The annual precipitation is greater than 2000 mm, and approximately 90% of the precipitation occurs during the summer when southwesterly monsoon prevails and typhoons frequently pass. Over half of the summer rainfall comes from tropical typhoons which commonly bring intensive rainfall (>100 mm/d) for a few days (see spiky daily rainfall in Fig. 1D).

3. Sampling and methods

Core TYP-B was retrieved from the center of Dongyuan Lake in 2004. Yang et al. (2011) previously used 16 AMS ^{14}C dates on organic materials of wood and plant debris to establish the chronology of the entire core (14.5 m). For this study, we focused on the middle part of this core from 8.5 to 13.2 m, which is comparable to the last deglaciation and the Early Holocene. We added 12 radiocarbon dates for this specific period to obtain a better age model. To obtain higher temporal resolution analyses, we subsampled at 1-cm intervals so that a total of 460 sub-samples were obtained from this segment with an average temporal resolution of approximately 16 calendar years, which is adequate to reveal multi-decadal to centennial scale variations in paleoclimate.

For total carbon analysis, an aliquot of freeze-dried, ground bulk sediments was analyzed with a HORIBA model EMIA-220 V C/S analyzer at 1350 °C. Note that, there is a certain amount of wood debris present in some sections of this core, thus, we picked out and weighed these wood debris before the measurements. Here, we analyzed the total carbon content instead of organic carbon as a paleoclimate proxy because the concentrations of TOC and TC were highly correlated (Fig. 2, $r^2 = 0.97$, $n = 95$). On the other hand, independent analysis on clay minerals revealed that the core contained only a trace amount of carbonate (Yang et al., 2011). Thus, we use TC hereafter in this study.

Magnetic susceptibility (MS) was measured with a Bartington MS2 Susceptibility System mounted on an ASC auto-tracking rail. Samples were also taken at 1-cm intervals.

The isotopic compositions of organic carbon were measured at 2–5 cm intervals by using an elemental analyzer (EA2100 Carlo Erba) coupled with a Thermo Finnigan Deltaplus Advantage isotope ratio mass spectrometer (IRMS), as detailed in Kao et al. (2006, 2008). All the isotopic values are presented in standard δ -notation in per mil (‰) with respect to Pee Dee Belemnite (PDB) carbon. The reproducibility of the carbon isotope measurements is better than 0.2‰.

Major elements (Al, Na, Ca and K) were taken at 5-cm intervals and analyzed by using an ICP-OES (Optima 3200DV, Perkin-Elmer™ Instruments, Waltham, Massachusetts, United States) to assess the state of chemical weathering. The total digestion method has been reported by Hsu et al. (2003). The major element contents were converted into their stoichiometric oxides for further calculation.

The total sediment accumulation rate (SAR) and mass accumulation rate (MAR-TC) of total carbon were calculated by using the following formula:

$$\text{SAR (g cm}^{-2}\text{yr}^{-1}) = \text{DBD (g cm}^{-3}) \times \text{LSR (cm yr}^{-1}) \quad (1)$$

$$\text{MAR-TC (g cm}^{-2}\text{yr}^{-1}) = \text{SAR} \times \text{TC (\%)} \quad (2)$$

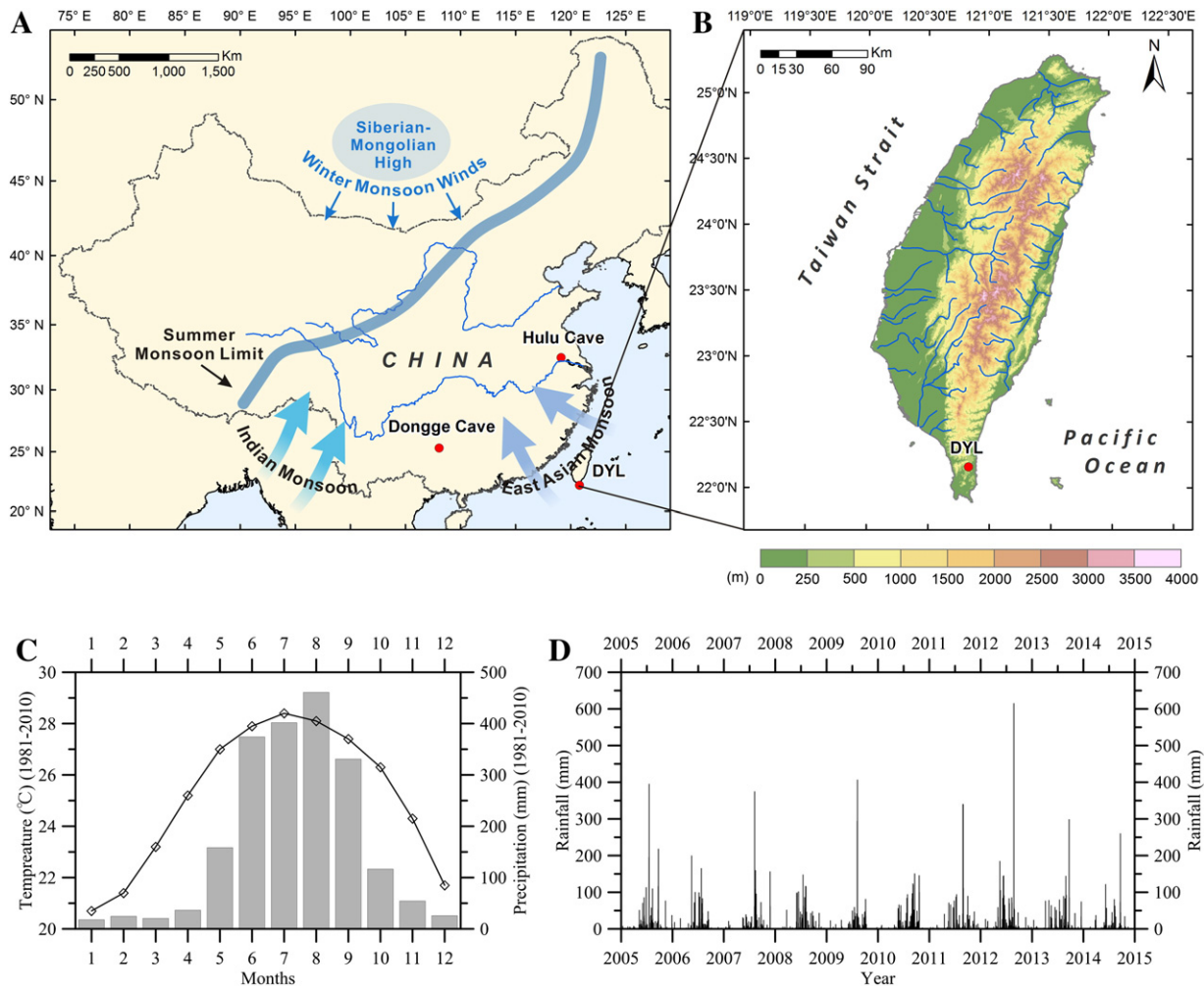


Fig. 1. Location and climatic data of the study area. (A) Asian monsoon region (modified from Selvaraj et al., 2012); (B) location of Dongyuan Lake (DYL) in Taiwan; (C) thirty-year mean monthly climatic records and (D) ten-year daily rainfall record from the Hengchun meteorological station near Dongyuan Lake (<http://www.cwb.gov.tw/>).

where DBD is the sediment dry bulk density and LSR is the linear sedimentation rate.

The chemical index of alteration (CIA) was calculated as in Nesbitt and Young (1982):

$$\text{CIA} = 100 \times \text{Al}_2\text{O}_3 / (\text{Al}_2\text{O}_3 + \text{Na}_2\text{O} + \text{CaO} + \text{K}_2\text{O}) \quad (3)$$

4. Results

4.1. Chronology and sedimentation rate

Table 1 shows the 16 radiocarbon dates including 4 dates previously used in Yang et al. (2011). Calibrated age ranges were converted by using the updated online calibration program Calib 702 (<http://calib.qub.ac.uk/calib/>, Reimer et al., 2013). Since there was a lack of plant debris in the section between 1010 cm and 1130 cm, two dates were assigned according to the bulk sediment at 1060 and 1097 cm. However, these two dates represent older ages relative to nearby dates on plant debris. The inverse ages indicated that the organic carbon associated with mineral soils may contain fossil/pre-aged organics, which has been commonly observed in suspended matter in Taiwan rivers (Hilton et al., 2011; Kao and Liu, 1996, 1997; Kao et al., 2014) and even in the Okinawa Trough, which receive sediments from Taiwan (Kao et al., 2008). Another two inverse dates on plant debris at 1180 cm and 1219 cm might be reworked wood. Excluding these 4

dates in the age–depth model shown in Fig. 3A, the chronology can be established by linear interpolation between each adjacent pair of calendar ages. The sedimentation rate during the investigated period was highly variable, ranging from ~0.2 mm/yr to ~2 mm/yr (Fig. 3B).

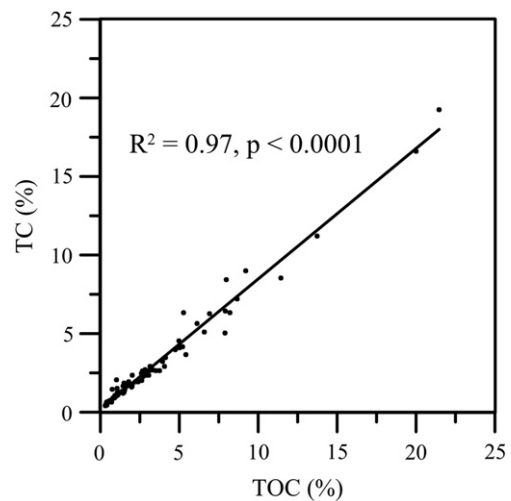


Fig. 2. Biplot of the total carbon content and against total organic carbon. The total organic carbon was reported by Yang et al. (2011).

Table 1

Radiocarbon dates for the period of investigation on TYP-B from Dongyuan Lake. Dates from previous study (Yang et al., 2011) are indicated by italics.

| Depth (cm) | Dating material | ^{14}C age (yr BP) | $\delta^{13}\text{C}$ (‰) | 2σ age range (yr cal BP) ^a | Lab. Code ^c |
|-------------------|-----------------|-----------------------------|---------------------------|--|------------------------|
| 868.5 | Plant debris | 8260 ± 35 | −28.3 | 9228 ± 103 | NZA29500 |
| 946 | Plant debris | 8627 ± 45 | −30.3 | 9607 ± 78 | NZA 33047 |
| 980 | Plant debris | 9229 ± 35 | −22.4 | 10,386.5 ± 117.5 | NZA29434 |
| 1010 | Plant debris | 9338 ± 35 | −26.3 | 10,573.5 ± 89.5 | NZA29438 |
| 1060 ^b | TOC | 10,690 ± 40 | −28.4 | 12,645.5 ± 70 | Beta−351,778 |
| 1097 ^b | TOC | 11,770 ± 60 | −30 | 13,601.5 ± 135 | Beta−351,779 |
| 1133.5 | Plant debris | 10,384 ± 40 | −28.4 | 12,238 ± 175 | NZA29498 |
| 1141 | Plant debris | 10,700 ± 55 | − | 12,646.5 ± 74.5 | WhOI OS-71,106 |
| 1153 | Plant debris | 11,014 ± 40 | −31.8 | 12,874 ± 129 | NZA30471 |
| 1170 | Plant debris | 11,400 ± 50 | − | 13,233.5 ± 117.5 | WhOI OS-71,106 |
| 1180 ^b | Plant debris | 11,941 ± 45 | −29.3 | 13,831.5 ± 135.5 | NZA29501 |
| 1217 | Plant debris | 11,716 ± 55 | −30.1 | 13,540 ± 104 | NZA33049 |
| 1219 ^b | Plant debris | 11,890 ± 46 | −30.5 | 13,677 ± 108 | NZA29503 |
| 1240 | Plant debris | 11,866 ± 55 | −28.3 | 13,669.5 ± 112.5 | NZA33050 |
| 1276 | Plant debris | 12,682 ± 45 | −27.7 | 15,073 ± 204 | NZA29497 |
| 1307 | Plant debris | 13,468 ± 50 | −27.7 | 16,211.5 ± 203.5 | NZA29499 |

^a All dates were calibrated with the Intcal13 dataset (Reimer et al., 2013).

^b Dates not used in the age–depth model (see in text).

^c Radiocarbon dating was measured at the Institute of Geological and Nuclear Sciences, New Zealand, Beta Analytic Inc. and Woods Hole Oceanographic Institution, USA.

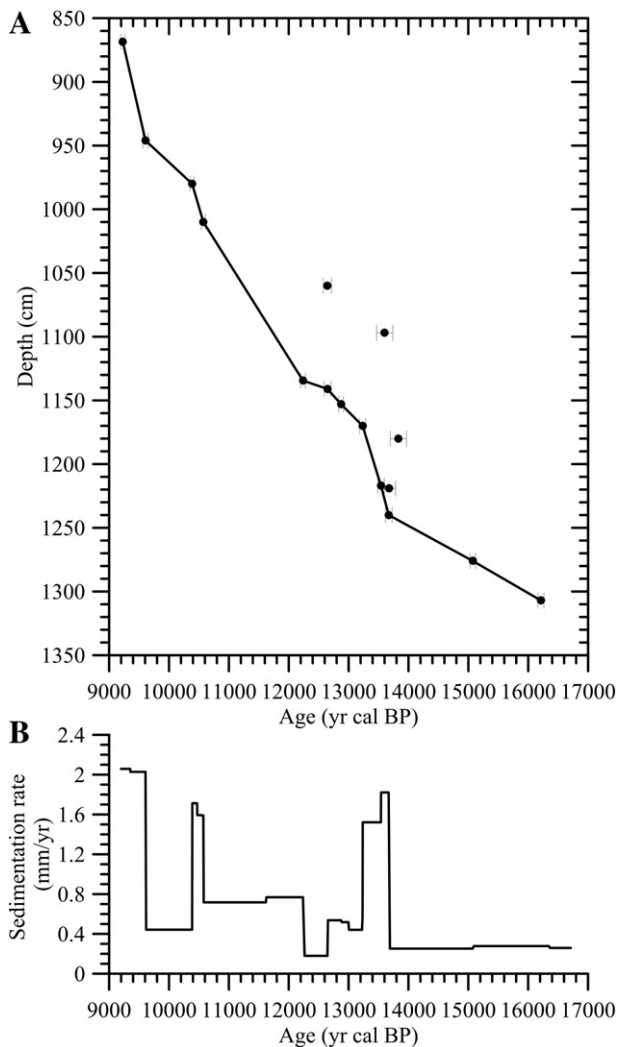


Fig. 3. Age–depth model (A) and sedimentation rate (B) for the investigated period of the core TYP-B.

Three distinct high sedimentation periods were 13.7–13.3 ka BP, 10.6–10.4 ka BP (1.5–1.8 mm/yr) and after 9.4 ka BP (~2 mm/yr). Such high sedimentation leads to high temporal resolution that a 1 cm sample may represent an integral of ~5 years to ~40 years, which is adequate to reveal centennial- and millennial- scale EASM variations.

4.2. Variations in lithology and multi-proxies

Fig. 4 shows the depth profile of multi-proxies (TC, TC-MAR, wood content, $\delta^{13}\text{C}_{\text{org}}$, MS, CIA, and Al_2O_3 content) measured in this study along with the lithology. The lithology of the core TYP-B exhibit alternations of layers of light gray or brown-gray muds and dark mud or interbedded mud. Generally, the lighter-colored mud layers coincided with low TC content, while the darker sections contained visible plant debris and higher TC content (Fig. 4). The most prominent feature of our record was the high-frequency and large-magnitude TC content and TC-MAR. Since TC and TC-MAR varied over 2 orders of magnitude, we applied log scale to reveal their fine variation structure (Fig. 4). In general, all the proxies coherently documented the occurrence of a series of abrupt climate changes during the investigated period (Fig. 4). The TC contents greatly fluctuated and varied between 0.35% and 19.25%, which reflects the instability of the climate in southern Taiwan during the last deglaciation. The temporal variation pattern of TC-MAR resembles that of TC. It should be noted that many plant remains occurred at depth of 1320–1310, 1230–1120, 100–980 and 880–860 cm. The $\delta^{13}\text{C}$ values fluctuated between −29.5‰ and −15.5‰. During most of the investigated period, the $\delta^{13}\text{C}$ exhibited depleted values (−29.5‰ to −26.5‰) and a light peak was evident occurred at the depth of 1100 cm (Fig. 4). The MS values generally varied opposite to the TC content. The CIA showed narrow but high values ranged between 82 and 85, which are comparable to alpine lake sediments as previously reported by Selvaraj and Chen (2006). The variation in Al_2O_3 content ranged from 12 to 20, which generally agrees with the MS record (Fig. 4).

5. Discussion

5.1. Significance and applications of the environmental proxies

The total organic carbon content in marine and lake sediments and loess/soil has been widely used as a proxy for the amount of precipitation (Meyers et al., 2006; Selvaraj et al., 2011; Xiao et al., 2006; Yang et al., 2011; Zhou et al., 2004). Higher TOC contents may infer larger inputs of eroded soil that is accompanied by plant debris due to enhanced monsoon intensity and vice versa. Thus we use the TC as a proxy for the EASM variability in this study. On the other hand, the mass accumulation rate of total organic carbon was suggested as a better measure of the delivery and preservation of organic matter than the TOC content (Meyers, 2003; Meyers and Lallier-Vergès, 1999). Accordingly, we also calculate the mass accumulation rate of TC for comparison.

In lake sediments, the $\delta^{13}\text{C}$ of organic carbon ($\delta^{13}\text{C}_{\text{org}}$) has been widely used to study the past vegetation and climate evolution (Li et al., 2013; Selvaraj et al., 2012; Xue et al., 2014; Zhang et al., 2011). Terrestrial plants that use the C_3 and C_4 pathways of photosynthesis have $\delta^{13}\text{C}$ values that range from −14‰ to −10‰ and from −30‰ to −22‰, respectively (O'Leary, 1981; Farquhar et al., 1989). It should be pointed out that the fossil organic carbon sourced from sedimentary bedrocks, which is commonly observed in the rivers and lakes in Taiwan, exhibits relatively constant $\delta^{13}\text{C}$ (−25‰, Hilton et al., 2010; Kao et al., 2014; Selvaraj et al., 2012). The autochthonous particulate organic matter in the surface water of Dongyuan Lake was mostly characterized by very negative $\delta^{13}\text{C}$ values (generally depleted than −29‰, Yang et al., 2011). However, the labile organics produced by algae can hardly be preserved due to the shallow depth of Dongyuan Lake and the strong vertical mixing of the lake water column, which is forced by frequent tropical cyclone and winter monsoon winds. According to the similarity in $\delta^{13}\text{C}_{\text{org}}$ between C_3 vegetation and lacustrine organics,

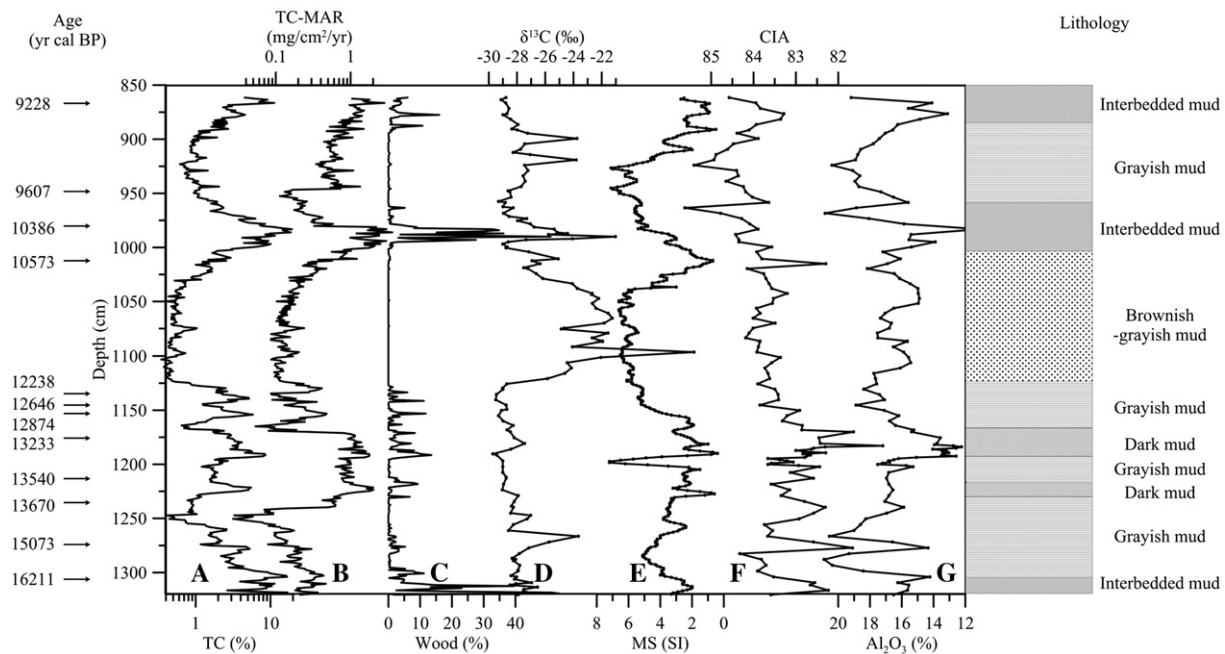


Fig. 4. Depth profile of multi-proxy data and lithology of sediment core from the Dongyuan Lake: (A) TC content; (B) mass accumulation rate of TC; (C) wood content; (D) $\delta^{13}\text{C}$ of the organic carbon; (E) magnetic susceptibility; (F) chemical index of alteration and (G) Al_2O_3 content. Note that the axis of MS, CIA and Al_2O_3 are reversed. Radiocarbon dates were also present with arrows.

we do not exclude the existence of autochthonous organics; however, the intimate and positive correlations among the amount of wood fragment, TC (or TOC) and published C/N ratios suggested that the majority of preserved organics were from allochthonous organics. Similar features have been observed in shallow lakes in Taiwan (e.g., Selvaraj et al., 2012). In this case, we suggest that the positive shift in $\delta^{13}\text{C}_{\text{org}}$ in the sediments from Dongyuan Lake was mainly influenced by C_4 plants from the catchment rather than autochthonous source.

On the other hand, the CIA defined by Nesbitt and Young (1982), was used to reconstruct the paleoclimate in drainage basins. CIA has been successfully applied as a measure of the chemical weathering status of a catchment. In Taiwan, however, active tectonics and typhoon events play important roles in regulating the local physical and chemical weathering processes (Goldsmith et al., 2008; Shao et al., 2012). The chemical weathering in Taiwan is relatively restricted because of the relatively short residence time of weathered soil due to frequent typhoon and storm-triggered erosion and even landslides on hillslopes (Selvaraj and Chen, 2006; Shao et al., 2012). As we know, vegetation cover exerts major control on soil erosion in mountainous watersheds in various climate zones and even in arid climate regions, such as the Loess Plateau (Zheng, 2006; Zhou et al., 2008). Higher vegetation cover may retain organics on the soil surface to prevent soil erosion; therefore, a longer soil residence time can be achieved. However, rainfall in Taiwan is episodic. The episodic rainfall results in luxurious vegetation in Taiwan, in the meantime, which creates more chances for gully rather than sheet erosion. The deeper soil and bedrock contain lower CIA values, which becomes more important during high precipitation periods instead due to gully erosion. This explains why the lower CIA is accompanied by a higher amount of organic debris in our record (Fig. 4).

The MS in lake sediments is often used as an indicator of catchment erosion and the transport and subsequent burial of clastic materials into lakes (Park et al., 2014; Selvaraj et al., 2007). Similarly, the Al_2O_3 content represents the intensity of detrital input into a lake catchment (Park et al., 2010, 2014). According to previous applications, high MS and Al_2O_3 values reflect increased erosion and deposition of minerogenic sediments under conditions of less vegetation cover and/or organic layer. In our case, the effect of organic dilution on the MS and Al_2O_3

content was evident; however, the amplitudes of the variation in both the MS and Al_2O_3 content (42% and 12%) were much smaller than the variability in organic contents (over 2 orders of magnitude), which preclude the sole control of organic input. Thus, the higher MS and Al_2O_3 values should indicate relatively intensified sheet erosion due to less vegetation cover caused by decreased precipitation during cool/dry periods and vice versa.

Another parameter, the wood fragment content, was proposed as a heavy rainfall index in this study. The wood fragment content has rarely been reported in the literature. Heavy rainfall (probably from tropical typhoons) and intensive wind might manipulate forest ecosystems. For example, typhoons determine the mean tree height in forests of northern Taiwan and severe winds can blow off huge amounts of leaves (Lin et al., 2010). Meanwhile, large amounts of particulate organic carbon (e.g., wood fragments and leaves), even tree trunks, can be transported to lakes and oceans by rivers during typhoons (Hilton et al., 2008; West et al., 2011; Liu et al., 2012). In that case, wood fragments might reflect the rainfall intensity to some extent. Thus, we picked out and quantified visible wood fragment to infer the intensity of heavy rains.

5.2. The evolution of the EASM during the last deglaciation and the Early Holocene

The variations in the EASM evolution registered in our record during the last deglaciation broadly agreed with millennial and sub-millennial timescale events that were recorded in high-resolution ice core, stalagmites and marine sediment records from the Northern Hemisphere (Fig. 5). The consistency indirectly demonstrates that our record faithfully tracked the EASM during the last deglaciation and that the strength of EASM in the study area is controlled by common forcings. The climate anomalies in the North Atlantic region have previously been proposed to be responsible for most of the variability in the EASM on millennial timescales via changes in the Atlantic Meridional Overturning Circulation (AMOC) and migration of the annual mean position of the Inter-tropical Convergence Zone (ITCZ) (Cheng et al., 2012). However, some subtle but significant discrepancies in millennial-scale events between Asian monsoon and Greenland temperature records have been

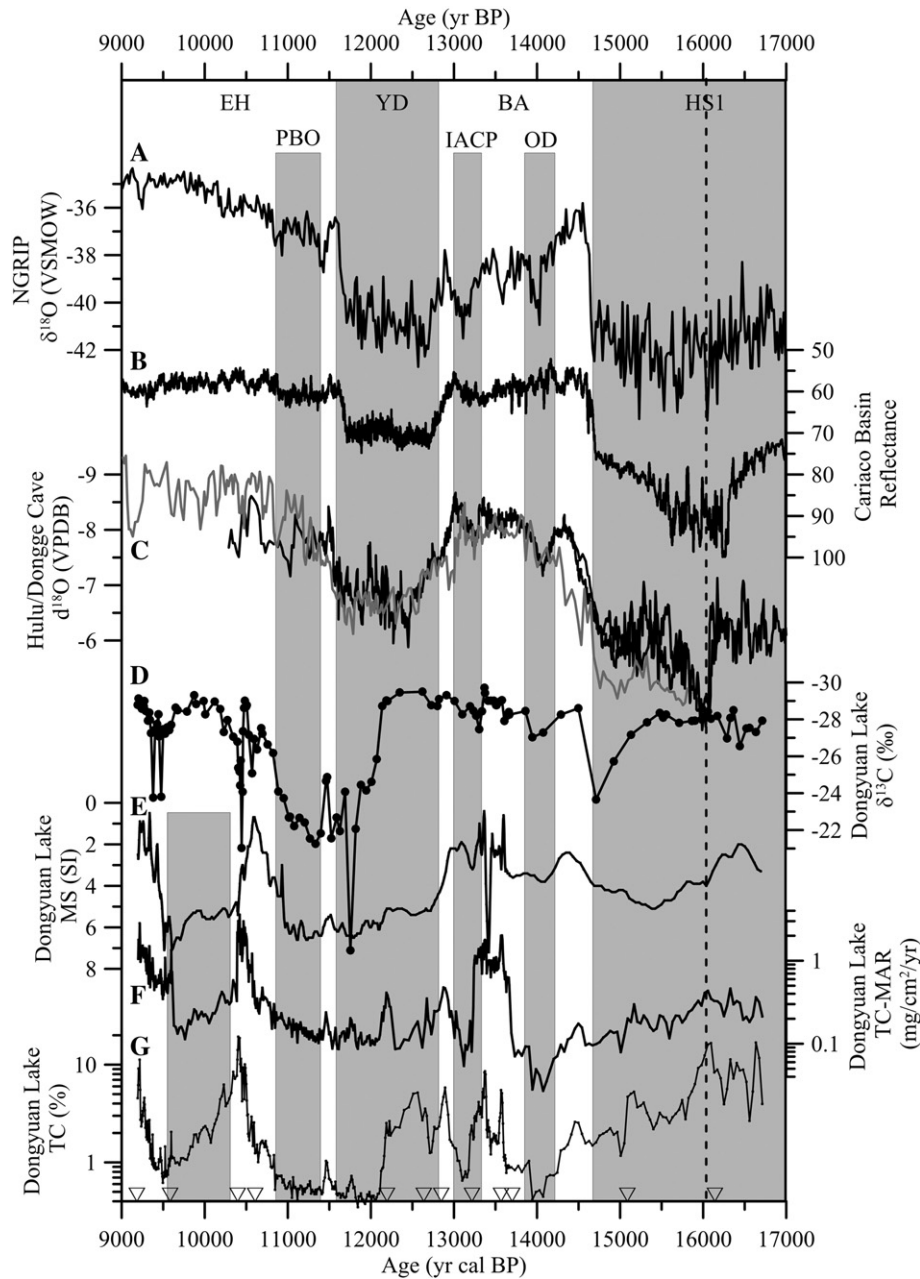


Fig. 5. Comparison of Dongyuan Lake records with other selected proxy records from Northern Hemisphere: (A) NGRIP $\delta^{18}\text{O}$ record (Andersen et al., 2006); (B) sediment reflectance record from Cariaco Basin, Venezuela (Deplazes et al., 2013); (C) stalagmite $\delta^{18}\text{O}$ record from Hulu Cave stalagmite (black, Wang et al., 2001) and Dongge Cave (grey, Dykoski et al., 2005) and (D–G) proxies from Dongyuan Lake, same as in Fig. 4 (this study). EH is Early Holocene, YD is Younger Dryas, BA is Bølling-Allerød, HS1 is Heinrich Stadial 1, PBO is Preboreal Oscillation, IACP is intra-Allerød cold period, OD is Older Dryas. Gray bars highlight the weak EASM intervals. Triangles represent the radiocarbon dates.

observed such as the mid-MI transition, BA trend and BA–YD transition (Liu et al., 2008; Liu et al., 2013; Ma et al., 2012; Shakun et al., 2007; Shen et al., 2010; Zhang et al., 2014), which probably indicates that other dynamics or regional scale processes are involved. Details of these events are discussed below.

5.2.1. During the Mystery Interval (17–14.7 ka BP)

The so-called Mystery Interval (Heinrich stadial 1) had been defined by Denton et al. (2006) based on many mutually contradictory characteristics across the globe (Denton et al., 2006; Broecker and Putnam, 2012; Zhang et al., 2014). During the Mystery Interval, prolonged cold conditions prevailed over the North Atlantic region associated with a collapse of the Atlantic Meridional Overturning Circulation (AMOC) (McManus et al., 2004), resulting in large meltwater discharge into the North Atlantic (Cheng et al., 2009). The reduction of AMOC, accordingly,

decreased the northward transportation of heat from low latitudes and increased sea ice coverage at northern high latitudes (Cheng et al., 2009). Meanwhile, the westerly wind belts shifted southward, and the atmospheric CO_2 concentrations and temperature in the Antarctic increased (Anderson et al., 2009; Jouzel et al., 2007). In this case, the mean position of the ITCZ shifted to the south and weakened the EASM. An analogous scenario to the Mystery Interval was also visible in earlier ice age terminations (Broecker et al., 2010; Cheng et al., 2009), which suggests the key role of monsoon systems in increasing atmospheric CO_2 concentrations and global warming during ice age terminations.

According to the variability of parameters in our record, the Mystery Interval can be separated into two phases (Fig. 5). During the early Mystery Interval (17–16.1 ka BP), the higher TC and greater amounts of plant debris suggest a climate with relatively high precipitation

intensity. The depleted $\delta^{13}\text{C}$ values (-26.5% – -28.4%) reflect the C_3 plant dominance in the catchment, while the lower values of MS, Al_2O_3 content and CIA (Figs. 4 and 5) indicate reduced erosion due to thick vegetation cover. While during the second half of MI (16.1–14.7), the TC significantly decreased, which might reflect decreased precipitation relative to the early MI. Higher MS and Al_2O_3 content might suggest an increase in mineral erosion due to sparse vegetation cover. The gradual increase in $\delta^{13}\text{C}$ values may indicate more contribution from C_4 plants (Fig. 5). All parameters in the later MI indicated a decreasing precipitation.

Precisely dated stalagmite records from central and eastern China revealed an abrupt weakening in the EASM at 16.1 ka (Fig. 5; Wang et al., 2001; Zhang et al., 2014). Meanwhile, an abrupt strengthening of the Indo-Australian summer monsoon (IASM) in the southern hemisphere was observed from the Ball Gown Cave in tropical Australia (Denniston et al., 2013). Such synchronous climatic shifts might indicate the southward migration of the ITCZ at 16.1 ka BP. Moreover, a major expansion of Lake Estancia in New Mexico in western U.S. occurred at 16.1 ka BP (i.e., Big Dry to Big Wet transition, Broecker and Putnam, 2012). Broecker and Putnam (2012) have suggested that this transition appears to be a part of a global hydrological reorganization. This abrupt shift of ITCZ, in fact, is directly related to the iceberg discharge maximum that was recorded in the North Atlantic (Stern and Lisiecki, 2013); however, the temperatures in Greenland did not cool further since the AMOC was already in the stadial mode during the first half of the MI (Zhang et al., 2014). That is why there was no corresponding shift in Greenland's $\delta^{18}\text{O}$ records (Fig. 5). Apparently, the two-phase transition in the EASM might not be simply explained by a stand-alone oceanic mechanism (Zhang et al., 2014).

A further southward displacement of the ITCZ and polar jet stream might be responsible for the significant transition during the mid-Mystery Interval (Zhang et al., 2014). In general, the polar jet stream shifts southward accompanying the ITCZ during boreal cold periods. The southward shift in the polar jet stream might modulate the position of the winter storm track and result in higher annual precipitation in the southwestern U.S. (Asmerom et al., 2010). This hypothesis was also supported by the reflectance value in the Cariaco Basin record, which shows the lowest value at 16.2 ka and indicates the most pronounced southward migration of the ITCZ (Fig. 5, Deplazes et al., 2013).

5.2.2. During the BA (14.7–12.7 ka BP)

Our records show dramatic oscillation during the BA, which suggests the instability of the paleoclimate in southern Taiwan. Similar fluctuations were also reported in other Asian monsoon regions (Hong et al., 2014; Park et al., 2014; Park and Park, 2015; Zhong et al., 2010). Numerous studies have reported that the BA was interrupted by several centennial-scale cold stadials including the OD and IACP. Stalagmite records also revealed the presence of these centennial-scale oscillations in the East Asian region during the BA (Fig. 5, Dykoski et al., 2005; Wang et al., 2001). However, few studies show clear correlation between lacustrine records in Taiwan and temperature oscillation in Greenland and stalagmite data. Our records are likely correlated with the Greenland temperature and cave records during these short-term stadials with larger amplitudes.

We observed a rapid depletion in $\delta^{13}\text{C}$ at the beginning of the BA, which was attributable to the increase in organic input from C_3 plants due to climate amelioration. Meanwhile, the gradual decrease in MS, CIA and Al_2O_3 content may imply a reduction in erosion due to increased vegetation cover on the catchment. The above four parameters responded more timely during the transition into the BA, but the carbon related parameters (TC, TC-MAR and wood content) and sedimentation rate revealed a delayed response with a dramatic increase at 13.7 ka BP (Figs. 4 and 5).

In fact, not only the delayed response in our record but many serious inconsistencies in climatic trends have also been observed between the Greenland ice core record and stalagmite EASM records, although both

fluctuated synchronously. In Fig. 5, we can clearly see a decreasing trend in Greenland's temperature after the very first jump while there was an increasing trend in EASM records throughout the BA. This discrepancy was attributed to the northern high latitudes climate, which had a limited effect on climate change at low latitudes during the BA. Similar discrepancies were also observed during earlier interstadials (Shakun et al., 2007; Shen et al., 2010). Thus, other forcing mechanisms such as Southern Hemisphere cooling (Antarctic cold reversal) or increasing Northern Hemisphere summer insolation, have been proposed to reconcile the inconsistency during the BA (Ma et al., 2012; Shakun et al., 2007; Shen et al., 2010). In any case, the intrinsic mechanism for the decoupling between tropical climatic records and North Atlantic climate records during the BA or earlier BA-like interstadials might require further exploration. Nevertheless, a variety of Asian monsoon proxy records compiled by Hong et al. (2014) suggested that the maximum rainfall or effective moisture in the Asian monsoon area did not occur during the Bølling but during the Allerød period.

The sharp decrease in TC and TC-MAR during the OD and IACP suggest decreased terrestrial organic matter input (Fig. 5). Slightly increased $\delta^{13}\text{C}$ and MS imply the proliferation of C_4 vegetation and decreased vegetation cover on the catchment due to environment deterioration (Fig. 5). The good correlation of these centennial-scale climate reversals between our records and Greenland's temperature further support the teleconnection between the North Atlantic and the low latitude East Asian region during the last deglaciation.

Note that, the variations of $\delta^{13}\text{C}$, MS, CIA and Al_2O_3 content were more consistent with Greenland's temperature, but the carbon content-associated parameters were not. We speculate that the carbon content was determined by relative intensity of supply and decomposition. Since the supply of wood debris reflects more events with torrential rain and intensive wind, which are mainly associated with typhoon frequency and intensity; therefore, the observed wood fragment peaks were likely caused by frequent typhoon events.

5.2.3. During the YD (12.7–11.5 ka BP)

Although the triggering mechanism is still controversial, the Younger Dryas event is the most well studied millennial-scale cold stadial during the last glacial period (Broecker et al., 2010). During the YD, the temperature over central Greenland dropped to full glacial conditions, about 15°C lower than today (Severinghaus et al., 1998). This cooling had a profound impact on climate systems beyond the North Atlantic regions (Clark et al., 2002; Shakun and Carlson, 2010). Stalagmite records over China show a significantly weakened EASM during the YD event starting at 12.9 ka BP (Dykoski et al., 2005; Liu et al., 2013; Ma et al., 2012; Wang et al., 2001).

In our records, again, the MS responded instantly (Fig. 5), whereas the TC and $\delta^{13}\text{C}$ exhibited a delayed response to the YD event, which shows dramatic change at 12.2 ka BP (Fig. 5). The decreased TC since 12.2 ka BP suggests decreased terrestrial organic matter input due to lower rainfall intensity. Enriched $\delta^{13}\text{C}$ ($> -24\%$ and up to -15%), which is higher than the $\delta^{13}\text{C}$ of rock (-25%), indicate that the sedimentary organic matter was mainly sourced from C_4 plants, although only in trace amounts. The extremely low TC contents (0.3%–0.8%) suggest that the organic decomposition during this period was much greater than the supply. The unprecedentedly low C/N (<5 , lower than the Redfield ratio for phytoplankton; Yang et al., 2011) also indicates a relatively complete organic decomposition with large portions of clay-fixed N in the remains (Zheng et al., 2015). During the same interval, the pollen records from Dongyuan Lake exhibit greater abundance of *Artemisia* (Lee et al., 2010). Since many *Artemisia* species use the C_4 pathway of photosynthesis and are usually abundant in arid or semiarid habitats (Jia et al., 2015), the pollen data further support a dry conditions during the late YD in southern Taiwan.

Interestingly, differing from the Greenland temperature records, the annually laminated stalagmite records from Qingtian Cave in central China show a gradual decrease in EASM during the early YD

(12.9–12.3 ka; Liu et al., 2013) instead of a rapid drop. This gentle decreasing trend is generally in agreement with other Asian monsoon records (Ma et al., 2012; Park et al., 2014; Shakun et al., 2007; Sinha et al., 2005; Yang et al., 2010). The inconsistency in the decreasing rate might suggest that other forcing mechanisms outside the North Atlantic region, such as an interference of the Southern Hemisphere climate via cross-equatorial air flow (Liu et al., 2008) or northward expanding low latitudinal warm currents (Park et al., 2014), modulated the EASM during the YD. The highly fluctuating TC and TC-MAR during the early YD likely illustrate that the feature of YD in mid-low latitudes, such as in Taiwan, was more like a gradual transition, which then resulted in prolonged vegetation type.

5.2.4. During the early Holocene (11.5–9 ka BP)

An abrupt decrease in oxygen isotope values at 11.6 ka marked the end of the YD in the stalagmite records (Fig. 5). Our records exhibit slight but significant increases in TC, TC-MAR and decrease in MS and $\delta^{13}\text{C}$, which indicate an amelioration (towards wet conditions) of the climate. However, immediately after the end of the YD, all the proxies showed a distinct climate deterioration (towards dry conditions), probably corresponding to the PBO (11.4–10.7 ka BP). A dramatic decline in monsoon activity during the PBO was not clearly observed in Chinese stalagmites (Fig. 5, Dykoski et al., 2005; Wang et al., 2001). From Fig. 5, we can see dramatic increases in sedimentation rate, TC, MAR-TC as well as concurrent amount of wood debris during 10.7–10.3 ka BP and after 9.4 ka BP. These parameter peaks indicate either a significantly increased denudation rate of the lake catchment induced by heavy precipitation, or engulfment of trees by elevating lake water level due to frequent and intense episodic typhoons (Selvaraj et al., 2011; Yang et al., 2011). Again, the lower MS, CIA, and $\delta^{13}\text{C}$ indicate a drastic reduction in detrital input to the lake due to thick vegetation (Figs. 4 and 5).

The climate deterioration during 10.3–9.4 ka BP has rarely been reported. It is difficult to give a reliable mechanism for such a dramatic climate deterioration in tropical Taiwan with copious precipitation result from the EASM and tropical cyclones during the Early Holocene. It happens that a dry event was observed 9.7–9.2 ka BP in the peat sequence from Toushe Basin in central Taiwan (Li et al., 2013; Liew et al., 2006b). This dry climatic reversal has also been reported in several published records from Asian monsoon region within the age uncertainty. For example, Chabangborn and Wohlfarth (2014) suggested that the mainland of Southeast Asia, which is also deeply influenced by tropical cyclones, experienced a warmer/dry climate between 10 and 9 ka BP after a cool/wet climatic conditions between 10.5 and 10 ka BP. Furthermore, Cook et al. (2013) suggested an unstable catchment environment and dry climate from 10.7 to 10.1 ka BP. Additionally, several studies from the Tibetan Plateau also suggested that a dry reversal occurred around 10 ka BP (An et al., 2012; Bird et al., 2014; Mischke and Zhang, 2010; Sun et al., 2015). According to the most recent report by Sun et al. (2015), we suggested that the dry reversal in the Asian summer monsoon at around 10 ka BP might be correlated with abrupt cooling in the North Atlantic, which is characterized by an ice-rafted debris event at 10.3 ka BP (Bond et al., 2001).

To our knowledge, the abrupt intensification of the EASM at 9.4 ka has not been seriously distinguished in any stalagmite records. By contrast, this intensification was highlighted in lacustrine and pollen records. For example, Jia et al. (2015) reported a marked enhancement of the EASM that was recorded in Huguangyan Maar Lake from southern China at 9.2 ka. Based on pollen assemblages, Zhao et al. (2009) indicated that environmental moisture during the first two millennia during the Holocene remained relatively low and reached a maximum until 9.5 ka BP. The broad consistency of these records suggest that a pronounced intensification of EASM did occur at 9.4 ka. Note that this time period coincides with the flooding of the Sunda shelf (~9.5 ka, Linsley et al., 2010). Although the intrinsic correlation between these two events remains unclear, the flooding of the Sunda shelf during the

Meltwater Pulse-1C (MWP-1C) reopened the semi-enclosed South China Sea (Linsley et al., 2010). The significant expansion of tropical water on the Sunda shelf probably helped to enhance the EASM (Jia et al., 2015).

The distinctive temporal evolution of EASM rainfall in our record during the Early Holocene suggests that the monsoonal rainfall on Taiwan Island was controlled by more complex dynamics. The decoupling between our record and northern high latitudes during the last deglaciation since the Holocene suggests a dampened influence of North Atlantic climate variability on the EASM due to decreasing sea ice cover and enhanced influence from tropical region. Similar transition had been observed in IASM system (Denniston et al., 2013). The hydrological variation and dynamics of the EASM rainfall in Taiwan deserve further studies in the future.

5.3. Possible links to the western tropical Pacific

Ocean–atmospheric interactions in the tropical Pacific have a strong influence on the export of heat and water vapor to high latitudes and therefore exert a significant control on global climate change (Lea, 2000). However, the role of forcing from the western tropical Pacific on the EASM in the past remained unclear due to a lack of high-resolution climate records in the Asia–Oceania region (Selvaraj et al., 2011). Cai et al. (2010) suggested that the variations of the SST in the western tropical Pacific might impact summer monsoon precipitation changes in central China and northern China since it affects the North-western Pacific High. Based on multiple proxies in sediment core from the subalpine Retreat Lake in northeastern Taiwan, Selvaraj et al. (2011) found a link between weakened EASM and the SST in the tropical Pacific. The authors suggested that the centennial-scale reorganizations in the tropical Pacific climate dynamics may have played an important role in the instability of EASM during the late Holocene. Recently, a study of Lake Huguangyan in southern China revealed an arid–wet–arid pattern in the EASM during the Holocene (Jia et al., 2015) that was in-phase with the hydrological variability in tropical Australia and anti-phase with that in the outer-tropical Andes. The authors attributed the variation pattern to the changes in the thermal state of the tropical Pacific. Nevertheless, documents of the links between the rainfall amount of the EASM and the variation of SST in the tropical Pacific during the last deglaciation remain limited.

Here, we compare our proxies with one of the highest resolution SST records from the western tropical Pacific (Rosenthal et al., 2003) (Fig. 6). Due to more complex forcing mechanisms on the EASM and multiple controls on organic carbon burial, the general pattern was different. Nevertheless, we found a serial centennial-scale distinct wet events (two exceptions at 14 ka and 10.5 ka) were in concert with distinct warm events in the western tropical Pacific (Fig. 6), which indicates an inherent connection between the western tropical Pacific SST and the variations of precipitation in Southern Taiwan. The enhancement of the monsoon convection resulting from increased SST in the western tropical Pacific likely increased the meridional heat transport from tropical to high latitudes. Modern meteorological data support this notion: high SST in the western tropical Pacific intensifies the upper-level convection from the Philippines to the Sino-India Peninsula via the South China Sea. Such intensification would force the subtropical high to move northward over East Asia and consequently shift the monsoon front and rain band northward (Huang et al., 2004). However, this is not a one-way process. Although the SST of the western tropical Pacific can influence the East Asian Monsoon climate, the monsoon climate might have feedbacks on the SST in the western tropical Pacific Ocean through altering the sea surface latent heat fluxes (Wang et al., 2003). Because of complicated oceanic–atmospheric interactions, we cannot conclude a causal relationship between the EASM precipitation and the SST of the western tropical Pacific though the centennial-scale inherent connection was observed. Additionally, the SST peak in western tropical Pacific at 14 ka BP has no counterpart in our record. Meanwhile,

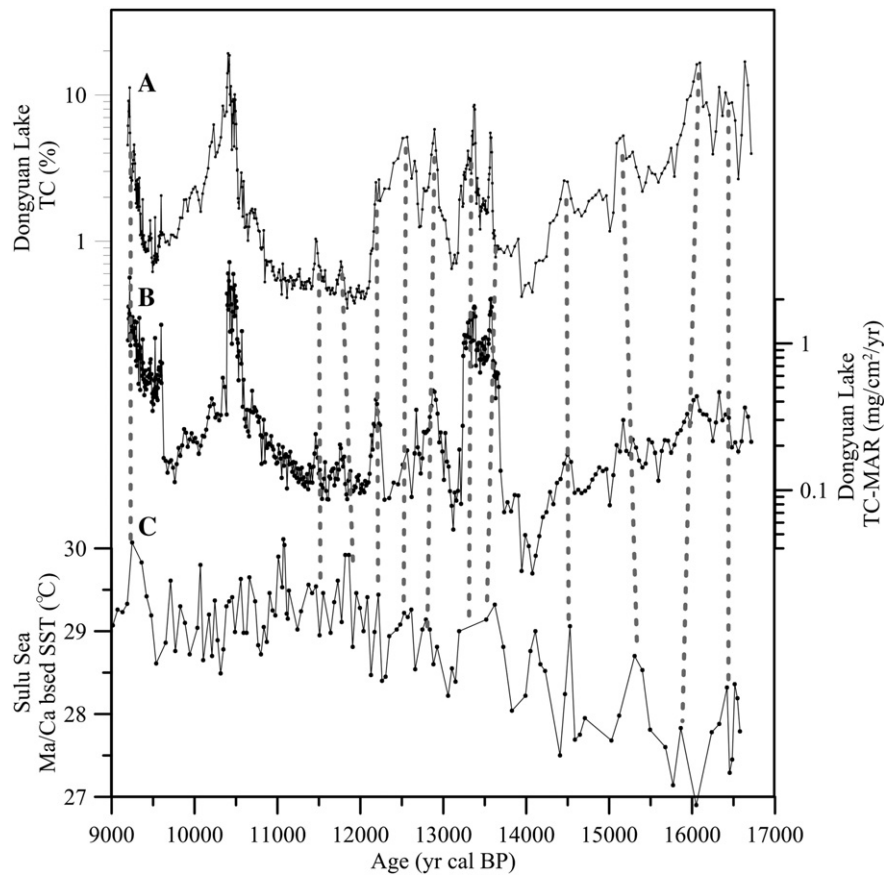


Fig. 6. Comparison of Dongyuan Lake records (A: TC, B: TC-MAR) with Mg/Ca-based SST records from western tropical Pacific (Rosenthal et al., 2003). Correlation of the distinct events is shown by the dashed line.

an extraordinary TC peak in our record at 10.5 ka BP was occurring at the plateau of SST in the western Pacific. More high-resolution records and robust tests are needed to confirm the relationship between the SST in western tropical Pacific and the EASM precipitation at the centennial timescale. Nevertheless, our study sheds light on the fact that the SST in the western tropical Pacific might play an important role in modulating the variation of the EASM.

5.4. Comparison with mass-wasting records from Taiwan

Since the content of wood fragment reflects typhoon impact, we compared our paleoclimatic data with the known mass-wasting records during the last deglaciation and the Early Holocene compiled by Hsieh et al. (2014) (Fig. 7). Large fan-terraces deposited after massive landslides or debris flow events have been noted in both southwestern and eastern Taiwan during the Early Holocene (Hsieh et al., 2011, 2012, 2014; Hsieh and Chyi, 2010). Mass-wasting events could be triggered by large earthquakes or heavy rainfall (Hsieh et al., 2014). It is not easy to decipher the forcing between earthquakes and climate data yet. Although different catchments have distinct mass-wasting histories, some of the recorded mass-wasting events among catchments do appear to have occurred synchronously (Fig. 7; Hsieh et al., 2014). The coincidence of the ages of the terraces constructed among different landforms prefer climatic than seismic forcing for the genesis of these mass-wasting records (Hsieh et al., 2014). Although a clear relationship between the mass-wasting sequences and our climatic records is difficult to find (Fig. 7), we notice that the largest mass-wasting activities recorded among these catchments occurred during 11.3–10.0 ka BP and 9.4–8.7 ka BP, which appeared correspondingly as the high sedimentation rate, TC and wood debris during 10.7–10.3 ka BP and after 9.4 ka BP in our record (Fig. 7). Kao et al. (2008) also reported an enhanced supply

of fossil organic carbon from Taiwan to the Okinawa Trough during the same periods. An extremely high sedimentation rate (~1.7 m/ka) was observed around 10.5 ka BP in the southern Okinawa Trough (Kao et al., 2008), which received sediments largely sourced from Taiwan. The synchronicity among independent observations from terraces, lake and marine sediments might suggest climatic conditions such as prolonged heavy rainfall due to increased frequency and/or intensity of tropical cyclones. These two peaks in our records and the greatest mass activities at the maximum insolation and the SST plateau in the western tropical Pacific (Linsley et al., 2010; Stott et al., 2004). Webster et al. (2005) reported that both the frequency and intensity of typhoons increase when tropical ocean SSTs increase. It is likely that the highest solar insolation and western tropical Pacific SSTs during the Early Holocene led to more frequent and more intense typhoons.

6. Conclusions

A 5- to 40-year resolution multi-proxy lacustrine record from Taiwan in southeast Asia provided detailed information of the EASM intensity during the last deglaciation and Early Holocene (17–9 ka BP). We compare this high-resolution record with stalagmite and ice core records from the Northern Hemisphere, specifically for millennial and centennial timescale climate events. Although the oscillation of the EASM intensity from our record generally coincided with the variation of North Atlantic climate at millennial scales, some subtle but significant discrepancies between our record and the Greenland ice core record (i.e., mid-MI transition, the BA trend with maximum monsoonal rainfall and the more gradual Allerød–YD transition in EASM intensity) suggested that the EASM intensity was influenced by a combination of AMOC variation and other forcing mechanisms (i.e., Southern Hemisphere climate, low-latitude warm current). A possible linkage

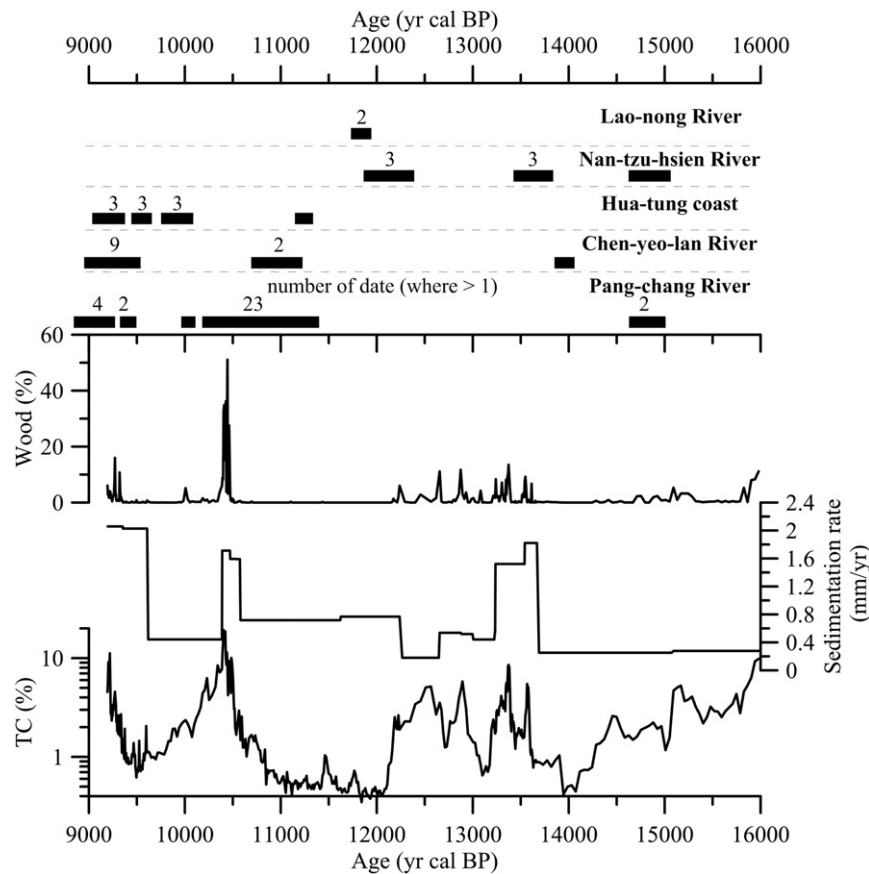


Fig. 7. Comparison of paleoclimatic data in this study with ancient mass-wasting records in Taiwan. The upper panel shows the available radiocarbon dates derived from mass-wasting sequences compiled by Hsieh et al. (2014). Bars represent 1σ calibrated ranges or their combinations where more than one set of data are available. The numbers (>1) of the dates are shown above the bars. The lower panel shows the climatic proxies from Dongyuan Lake in this study.

between EASM and SST in western tropical Pacific at the centennial timescale was observed, which suggests that the reorganizations in tropical Pacific climate dynamic might have impacted on EASM precipitation in Taiwan. In addition, we found pronounced high sedimentation events accompanied by an amount of wood fragment burial in the lake sediments during the Early Holocene, which were synchronous with the largest mass-wasting records in river channels from Taiwan and deposition peaks in the southern Okinawa Trough. The synchronicity among lacustrine, river channel and marine deposits probably indicated that heavy rainfall from tropical cyclones had prevailed during these periods. These observations call for further studies about the dynamics of EASM rainfall in Southeast Asia that co-influenced by the EASM and typhoon activities.

Acknowledgments

We sincerely thank the editor and the anonymous reviewers for their constructive comments and suggestions for improving the manuscript. We would like to thank Dr. T.Y. Lee at NTNU, Taiwan for the artwork. This research was supported by the Natural Science Foundation of China (41176059; 91328207).

References

An, Z., 2000. The history and variability of the East Asian paleomonsoon climate. *Quat. Sci. Rev.* 19, 171–187.
 An, Z., Colman, S.M., Zhou, W., Li, X., Brown, E.T., Jull, A.J., Cai, Y., Huang, Y., Lu, X., Chang, H., Song, Y., Sun, Y., Xu, H., Liu, W., Jin, Z., Liu, X., Cheng, P., Liu, Y., Ai, L., Li, X., Liu, X., Yan, L., Shi, Z., Wang, X., Wu, F., Qiang, X., Dong, J., Lu, F., Xu, X., 2012. Interplay between the westerlies and Asian monsoon recorded in Lake Qinghai sediments since 32 ka. *Sci. Rep.* 2, 619.

Andersen, K.K., Svensson, A., Johnsen, S.J., Rasmussen, S.O., Bigler, M., Röthlisberger, R., Ruth, U., Siggaard-Andersen, M.-L., Steffensen, J.P., Dahl-Jensen, D., 2006. The Greenland ice core chronology 2005, 15–42 ka. Part 1: Constructing the time scale. *Quat. Sci. Rev.* 25, 3246–3257.
 Anderson, R.F., Ali, S., Bradtmiller, L.L., Nielsen, S.H.H., Fleisher, M.Q., Anderson, B.E., Burckle, L.H., 2009. Wind-driven upwelling in the Southern Ocean and the deglacial rise in atmospheric CO_2 . *Science* 323, 1443–1448.
 Asmerom, Y., Polyak, V.J., Burns, S.J., 2010. Variable winter moisture in the Southwestern United States linked to rapid glacial climate shifts. *Nat. Geosci.* 3, 114–117.
 Bird, B.W., Polisar, P.J., Lei, Y., Thompson, L.G., Yao, T., Finney, B.P., Bain, D.J., Pompeani, D.P., Steinman, B.A., 2014. A Tibetan lake sediment record of Holocene Indian summer monsoon variability. *Earth Planet. Sci. Lett.* 399, 92–102.
 Bond, G., Kromer, B., Beer, J., Muscheler, R., Evans, M.N., Showers, W., Hoffmann, S., Lotti-Bond, R., Hajdas, I., Bonani, G., 2001. Persistent solar influence on North Atlantic climate during the Holocene. *Science* 294, 2130–2136.
 Broecker, W., Putnam, A.E., 2012. How did the hydrologic cycle respond to the two-phase mystery interval? *Quat. Sci. Rev.* 57, 17–25.
 Broecker, W.S., Denton, G.H., Edwards, R.L., Cheng, H., Alley, R.B., Putnam, A.E., 2010. Putting the Younger Dryas cold event into context. *Quat. Sci. Rev.* 29, 1078–1081.
 Cai, Y., An, Z., Cheng, H., Edwards, R.L., Kelly, M.J., Liu, W., Wang, X., Shen, C.-C., 2006. High-resolution absolute-dated Indian monsoon record between 53 and 36 ka from Xiaobailong Cave, Southwestern China. *Geology* 34, 621–624.
 Cai, Y., Tan, L., Cheng, H., An, Z., Edwards, R.L., Kelly, M.J., Kong, X., Wang, X., 2010. The variation of summer monsoon precipitation in Central China since the last deglaciation. *Earth Planet. Sci. Lett.* 291, 21–31.
 Chabangborn, A., Wohlfarth, B., 2014. Climate over mainland Southeast Asia 10.5–5 ka. *J. Quat. Sci.* 29, 445–454.
 Chen, C.-S., Chen, Y.-L., 2003. The rainfall characteristics of Taiwan. *Mon. Weather Rev.* 131, 1323–1341.
 Chen, J.-M., Li, T., Shih, C.-F., 2010. Tropical cyclone- and monsoon-induced rainfall variability in Taiwan. *J. Clim.* 23, 4107–4120.
 Cheng, H., Edwards, R.L., Broecker, W.S., Denton, G.H., Kong, X., Wang, Y., Zhang, R., Wang, X., 2009. Ice age terminations. *Science* 326, 248–252.
 Cheng, H., Edwards, R.L., Wang, Y., Kong, X., Ming, Y., Kelly, M.J., Wang, X., Gallup, C.D., Liu, W., 2006. A penultimate glacial monsoon record from Hulu Cave and two-phase glacial terminations. *Geology* 34, 217–220.
 Cheng, H., Sinha, A., Wang, X., Cruz, F.W., Edwards, R.L., 2012. The global paleomonsoon as seen through speleothem records from Asia and the Americas. *Clim. Dyn.* 39, 1045–1062.

- Clark, P.U., Piasis, N.G., Stocker, T.F., Weaver, A.J., 2002. The role of the thermohaline circulation in abrupt climate change. *Nature* 415, 863–869.
- Cook, C.G., Jones, R.T., Turney, C.S.M., 2013. Catchment instability and Asian summer monsoon variability during the early Holocene in Southwestern China. *Boreas* 42, 224–235.
- Denniston, R.F., Wyrwoll, K.-H., Asmerom, Y., Polyak, V.J., Humphreys, W.F., Cugley, J., Woods, D., LaPointe, Z., Peota, J., Greaves, E., 2013. North Atlantic forcing of millennial-scale Indo-Australian monsoon dynamics during the last glacial period. *Quat. Sci. Rev.* 72, 159–168.
- Denton, G.H., Broecker, W.S., Alley, R.B., 2006. The mystery interval 17.5 to 14.5 kyrs ago. *PAGES News* 14, 14–16.
- Deplazes, G., Lückge, A., Peterson, L.C., Timmermann, A., Hamann, Y., Hughen, K.A., Röhl, U., Laj, C., Cane, M.A., Sigman, D.M., Haug, G.H., 2013. Links between tropical rainfall and North Atlantic climate during the last glacial period. *Nat. Geosci.* 6, 213–217.
- Dykoski, C.A., Edwards, R.L., Cheng, H., Yuan, D., Cai, Y., Zhang, M., Lin, Y., Qing, J., An, Z., Revenaugh, J., 2005. A high-resolution, absolute-dated Holocene and deglacial Asian monsoon record from Dongge cave, China. *Earth Planet. Sci. Lett.* 233, 71–86.
- Farquhar, G., Ehleringer, J., Hubick, K., 1989. Carbon isotope discrimination and photosynthesis. *Annu. Rev. Plant Physiol.* 40, 503–537.
- Genty, D., Blamart, D., Ghaleb, B., Plagnes, V., Causse, C., Bakalowicz, M., Zouari, K., Chkir, N., Hellstrom, J., Wainer, K., 2006. Timing and dynamics of the last deglaciation from European and North African $\delta^{13}\text{C}$ stalagmite profiles—comparison with Chinese and South Hemisphere stalagmites. *Quat. Sci. Rev.* 25, 2118–2142.
- Goldsmith, S.T., Carey, A.E., Lyons, W.B., Kao, S.-J., Lee, T.Y., Chen, J., 2008. Extreme storm events, landscape denudation, and carbon sequestration: Typhoon Mindulle, Choshui River, Taiwan. *Geology* 36, 483.
- Hilton, R.G., Galy, A., Hovius, N., Chen, M.-C., Horng, M.-J., Chen, H., 2008. Tropical-cyclone-driven erosion of the terrestrial biosphere from mountains. *Nat. Geosci.* 1, 759–762.
- Hilton, R.G., Galy, A., Hovius, N., Horng, M.-J., Chen, H., 2010. The isotopic composition of particulate organic carbon in mountain rivers of Taiwan. *Geochim. Cosmochim. Acta* 74, 3164–3181.
- Hilton, R.G., Galy, A., Hovius, N., Horng, M.-J., Chen, H., 2011. Efficient transport of fossil organic carbon to the ocean by steep mountain rivers: an orogenic carbon sequestration mechanism. *Geology* 39, 71–74.
- Hong, B., Hong, Y., Uchida, M., Shibata, Y., Cai, C., Peng, H., Zhu, Y., Wang, Y., Yuan, L., 2014. Abrupt variations of Indian and East Asian summer monsoons during the last deglacial stadial and interstadial. *Quat. Sci. Rev.* 97, 58–70.
- Hsieh, M.-L., Chyi, S.-J., 2010. Late quaternary mass-wasting records and formation of fan terraces in the Chen-yeo-lan and Lao-nung catchments, Central-Southern Taiwan. *Quat. Sci. Rev.* 29, 1399–1418.
- Hsieh, M.-L., Ching, K.-E., Chyi, S.-J., Kang, S.-C., Chou, C.-Y., 2014. Late quaternary mass-wasting records in the actively uplifting Pa-chang catchment, Southwestern Taiwan. *Geomorphology* 216, 125–140.
- Hsieh, M.-L., Lai, L.S.-H., Lin, C.D.-J., Shyu, J.B.H., 2012. Late quaternary landscape evolution and genesis of the 2009 catastrophic landslide in the Hsiao-lin area, Southwestern Taiwan. *Geomorphology* 179, 225–239.
- Hsieh, M.-L., Liew, P.-M., Chen, H.-W., 2011. Early Holocene catastrophic mass-wasting event and fan-delta development on the Hua-tung coast, Eastern Taiwan. *Geomorphology* 134, 378–393.
- Hsu, S.-C., Lin, F.-J., Jeng, W.-L., Chung, Y.-c., Shaw, L.-M., 2003. Hydrothermal signatures in the Southern Okinawa Trough detected by the sequential extraction of settling particles. *Mar. Chem.* 84, 49–66.
- Huang, R., Huang, G., Wei, Z.G., 2004. Climate Variations of the Summer Monsoon over China. In: Chang, C.-P. (Ed.), *East Asian Monsoon*. World Scientific Publishing Co. Pte. Ltd, Singapore, pp. 213–268.
- Jia, G., Bai, Y., Yang, X., Xie, L., Wei, G., Ouyang, T., Chu, G., Liu, Z., Peng, P.a., 2015. Biogeochemical evidence of Holocene East Asian summer and winter monsoon variability from a tropical maar lake in Southern China. *Quat. Sci. Rev.* 111, 51–61.
- Jouzel, J., Masson-Delmotte, V., Cattani, O., Dreyfus, G., Falourd, S., Hoffmann, G., Minster, B., Nouet, J., Barnola, J.-M., Chappellaz, J., 2007. Orbital and millennial Antarctic climate variability over the past 800,000 years. *Science* 317, 793–796.
- Kao, S., Liu, K., 1997. Fluxes of dissolved and nonfossil particulate organic carbon from an Oceania small river (Lanyang Hsi) in Taiwan. *Biogeochemistry* 39, 255–269.
- Kao, S.-J., Liu, K.-K., 1996. Particulate organic carbon export from a subtropical mountainous river (Lanyang Hsi) in Taiwan. *Limnol. Oceanogr.* 41, 1749–1757.
- Kao, S.J., Milliman, J.D., 2008. Water and sediment discharge from small mountainous rivers, Taiwan: the roles of lithology, episodic events, and human activities. *J. Geol.* 116, 431–448.
- Kao, S.J., Dai, M.H., Wei, K.Y., Blair, N.E., Lyons, W.B., 2008. Enhanced supply of fossil organic carbon to the Okinawa Trough since the last deglaciation. *Paleoceanography* 23, 1–12.
- Kao, S.J., Hilton, R.G., Selvaraj, K., Dai, M., Zehetner, F., Huang, J.C., Hsu, S.C., Sparkes, R., Liu, J.T., Lee, T.Y., Yang, J.Y.T., Galy, A., Xu, X., Hovius, N., 2014. Preservation of terrestrial organic carbon in marine sediments offshore Taiwan: mountain building and atmospheric carbon dioxide sequestration. *Earth Surf. Dyn.* 2, 127–139.
- Kao, S.-J., Shiah, F.-K., Wang, C.-H., Liu, K.-K., 2006. Efficient trapping of organic carbon in sediments on the continental margin with high fluvial sediment input off Southwestern Taiwan. *Cont. Shelf Res.* 26, 2520–2537.
- Lea, D.W., 2000. Climate impact of Late Quaternary equatorial Pacific Sea surface temperature variations. *Science* 289, 1719–1724.
- Lee, C.-Y., Liew, P.-M., 2010. Late quaternary vegetation and climate changes inferred from a pollen record of Dongyuan Lake in Southern Taiwan. *Palaeogeogr. Palaeoclimatol. Palaeoecol.* 287, 58–66.
- Lee, C.Y., Liew, P.M., Lee, T.Q., 2010. Pollen records from Southern Taiwan: implications for East Asian summer monsoon variation during the Holocene. *The Holocene* 20, 81–89.
- Lee, C.-Y., Chang, C.-L., Liew, P.-M., Lee, T.-Q., Song, S.-R., 2014. Climate change, vegetation history, and agricultural activity of Lake Li-Yu Tan, Central Taiwan, during the last 2.6 ka BP. *Quat. Int.* 325, 105–110.
- Li, H.-C., Liew, P.-M., Seki, O., Kuo, T.-S., Kawamura, K., Wang, L.-C., Lee, T.-Q., 2013. Paleoclimate variability in Central Taiwan during the past 30 Kyrs reflected by pollen, $\delta^{13}\text{C}_{\text{TOC}}$, and *n*-alkane- δD records in a peat sequence from Toushe Basin. *J. Asian Earth Sci.* 69, 166–176.
- Li, Y.-H., 1976. Denudation of Taiwan Island since the Pliocene epoch. *Geology* 4, 105–107.
- Liew, P.M., Lee, C.Y., Kuo, C.M., 2006b. Holocene thermal optimal and climate variability of East Asian monsoon inferred from forest reconstruction of a subalpine pollen sequence, Taiwan. *Earth Planet. Sci. Lett.* 250, 596–605.
- Liew, P.-M., Huang, S.-Y., Kuo, C.-M., 2006a. Pollen stratigraphy, vegetation and environment of the last glacial and Holocene—a record from Toushe Basin, Central Taiwan. *Quat. Int.* 147, 16–33.
- Liew, P.-M., Wu, M.-H., Lee, C.-Y., Chang, C.-L., Lee, T.-Q., 2014. Recent 4000 years of climatic trends based on pollen records from lakes and a bog in Taiwan. *Quat. Int.* 349, 105–112.
- Lin, T.-C., Hamburg, S.P., Lin, K.-C., Wang, L.-J., Chang, C.-T., Hsia, Y.-J., Vadeboncoeur, M.A., Mabry McMullen, C.M., Liu, C.-P., 2010. Typhoon disturbance and forest dynamics: lessons from a Northwest Pacific subtropical forest. *Ecosystems* 14, 127–143.
- Linsley, B.K., Rosenthal, Y., Oppo, D.W., 2010. Holocene evolution of the Indonesian throughflow and the Western Pacific warm pool. *Nat. Geosci.* 3, 578–583.
- Liu, D., Wang, Y., Cheng, H., Edwards, R.L., Kong, X., Wang, X., Wu, J., Chen, S., 2008. A detailed comparison of Asian monsoon intensity and Greenland temperature during the Allerød and Younger Dryas events. *Earth Planet. Sci. Lett.* 272, 691–697.
- Liu, D., Wang, Y., Cheng, H., Kong, X., Chen, S., 2013. Centennial-scale Asian monsoon variability during the mid-Younger Dryas from Qingtian Cave, Central China. *Quat. Res.* 80, 199–206.
- Liu, J.T., Wang, Y.H., Yang, R.J., Hsu, R.T., Kao, S.J., Lin, H.L., Kuo, F.H., 2012. Cyclone-induced hyperpycnal turbidity currents in a submarine canyon. *J. Geophys. Res. Oceans* 117, 117.
- Liu, Z., Wen, X., Brady, E.C., Otto-Bliesner, B., Yu, G., Lu, H., Cheng, H., Wang, Y., Zheng, W., Ding, Y., Edwards, R.L., Cheng, J., Liu, W., Yang, H., 2014. Chinese cave records and the East Asia summer monsoon. *Quat. Sci. Rev.* 83, 115–128.
- Ma, Z.-B., Cheng, H., Tan, M., Edwards, R.L., Li, H.-C., You, C.-F., Duan, W.-H., Wang, X., Kelly, M.J., 2012. Timing and structure of the Younger Dryas event in Northern China. *Quat. Sci. Rev.* 41, 83–93.
- Maher, B.A., Thompson, R., 2012. Oxygen isotopes from Chinese caves: records not of monsoon rainfall but of circulation regime. *J. Quat. Sci.* 27, 615–624.
- McManus, J., Francois, R., Gherardi, J.-M., Keigwin, L., Brown-Leger, S., 2004. Collapse and rapid resumption of Atlantic meridional circulation linked to deglacial climate changes. *Nature* 428, 834–837.
- Meyers, P.A., 2003. Applications of organic geochemistry to paleolimnological reconstructions: a summary of examples from the Laurentian Great Lakes. *Org. Geochem.* 34, 261–289.
- Meyers, P.A., Lallier-Vergès, E., 1999. Lacustrine sedimentary organic matter records of late quaternary paleoclimates. *J. Paleolimnol.* 21, 345–372.
- Meyers, P.A., Bernasconi, S.M., Forster, A., 2006. Origins and accumulation of organic matter in expanded Albian to Santonian black shale sequences on the Demerara Rise, South American margin. *Org. Geochem.* 37, 1816–1830.
- Mischke, S., Zhang, C., 2010. Holocene cold events on the Tibetan Plateau. *Glob. Planet. Chang.* 72, 155–163.
- Nesbitt, H., Young, G., 1982. Early Proterozoic climates and plate motions inferred from major element chemistry of lutites. *Nature* 299, 715–717.
- O'Leary, M.H., 1981. Carbon isotope fractionation in plants. *Phytochemistry* 20, 553–567.
- Park, J., Park, J., 2015. Pollen-based temperature reconstructions from Jeju Island, South Korea and its implication for coastal climate of East Asia during the Late Pleistocene and Early Holocene. *Palaeogeogr. Palaeoclimatol. Palaeoecol.* 417, 445–457.
- Park, J., Byrne, R., Böhnell, H., Garza, R.M., Conserva, M., 2010. Holocene climate change and human impact, Central Mexico: a record based on maar lake pollen and sediment chemistry. *Quat. Sci. Rev.* 29, 618–632.
- Park, J., Lim, H.S., Lim, J., Park, Y.-H., 2014. High-resolution multi-proxy evidence for millennial- and centennial-scale climate oscillations during the last deglaciation in Jeju Island, South Korea. *Quat. Sci. Rev.* 105, 112–125.
- Pausata, F.S.R., Battisti, D.S., Nisancioglu, K.H., Bitz, C.M., 2011. Chinese stalagmite $\delta^{18}\text{O}$ controlled by changes in the Indian monsoon during a simulated Heinrich event. *Nat. Geosci.* 4, 474–480.
- Reimer, P.J., Bard, E., Bayliss, A., Beck, J.W., Blackwell, P.G., Ramsey, C.B., Grootes, P.M., Guilderson, T.P., Hafliadason, H., Hajdas, I., 2013. *IntCal13 and Marine13 radiocarbon age calibration curves 0–50,000 years cal BP*. *Radiocarbon* 55, 1869–1887.
- Rosenthal, Y., Oppo, D., Linsley, B., 2003. The amplitude and phasing of climate change during the last deglaciation in the Sulu Sea, western equatorial Pacific. *Geophys. Res. Lett.* 30, 1428.
- Selvaraj, K., Chen, C.T.A., 2006. Moderate chemical weathering of subtropical Taiwan: constraints from solid-phase geochemistry of sediments and sedimentary rocks. *J. Geol.* 114, 101–116.
- Selvaraj, K., Arthur Chen, C.-T., Lou, J.-Y., Kotlia, B.S., 2011. Holocene weak summer east Asian monsoon intervals in Taiwan and plausible mechanisms. *Quat. Int.* 229, 57–66.
- Selvaraj, K., Chen, C.T.A., Lou, J.Y., 2007. Holocene East Asian monsoon variability: links to solar and tropical Pacific forcing. *Geophys. Res. Lett.* 34, L01703.
- Selvaraj, K., Wei, K.-Y., Liu, K.-K., Kao, S.-J., 2012. Late Holocene monsoon climate of Northeastern Taiwan inferred from elemental (C, N) and isotopic ($\delta^{13}\text{C}$, $\delta^{15}\text{N}$) data in lake sediments. *Quat. Sci. Rev.* 37, 48–60.
- Severinghaus, J.P., Sowers, T., Brook, E.J., Alley, R.B., Bender, M.L., 1998. Timing of abrupt climate change at the end of the Younger Dryas interval from thermally fractionated gases in polar ice. *Nature* 391, 141–146.

- Shakun, J.D., Carlson, A.E., 2010. A global perspective on last glacial maximum to Holocene climate change. *Quat. Sci. Rev.* 29, 1801–1816.
- Shakun, J.D., Burns, S.J., Fleitmann, D., Kramers, J., Matter, A., Al-Subary, A., 2007. A high-resolution, absolute-dated deglacial speleothem record of Indian Ocean climate from Socotra Island, Yemen. *Earth Planet. Sci. Lett.* 259, 442–456.
- Shao, J., Yang, S., Li, C., 2012. Chemical indices (CIA and WIP) as proxies for integrated chemical weathering in China: inferences from analysis of fluvial sediments. *Sediment. Geol.* 265–266, 110–120.
- Shen, C.C., Kano, A., Hori, M., Lin, K., Chiu, T.C., Burr, G.S., 2010. East Asian monsoon evolution and reconciliation of climate records from Japan and Greenland during the last deglaciation. *Quat. Sci. Rev.* 29, 3327–3335.
- Sinha, A., Cannariato, K.G., Stott, L.D., Li, H.-C., You, C.-F., Cheng, H., Edwards, R.L., Singh, I.B., 2005. Variability of southwest Indian summer monsoon precipitation during the Bølling–Allerød. *Geology* 33, 813–816.
- Stern, J.V., Lisiecki, L.E., 2013. North Atlantic circulation and reservoir age changes over the past 41,000 years. *Geophys. Res. Lett.* 40, 3693–3697.
- Stott, L., Cannariato, K., Thunell, R., Haug, G.H., Koutavas, A., Lund, S., 2004. Decline of surface temperature and salinity in the western tropical Pacific Ocean in the Holocene epoch. *Nature* 431, 56–59.
- Sun, W., Zhang, E., Jones, R.T., Liu, E., Shen, J., 2015. Asian summer monsoon variability during the late glacial and Holocene inferred from the stable carbon isotope record of black carbon in the sediments of Muge Co, southeastern Tibetan plateau, China. *The Holocene* 25, 1857–1868.
- Wang, B., Wu, R., Li, T., 2003. Atmosphere–warm ocean interaction and its impacts on Asian–Australian monsoon variation*. *J. Clim.* 16, 1195–1211.
- Wang, L.-C., Behling, H., Chen, Y.-M., Huang, M.-S., Arthur Chen, C.-T., Lou, J.-Y., Chang, Y.-P., Li, H.-C., 2014. Holocene monsoonal climate changes tracked by multiproxy approach from a lacustrine sediment core of the subalpine retreat lake in Taiwan. *Quat. Int.*
- Wang, L.-C., Behling, H., Kao, S.-J., Li, H.-C., Selvaraj, K., Hsieh, M.-L., Chang, Y.-P., 2015. Late Holocene environment of subalpine Northeastern Taiwan from pollen and diatom analysis of lake sediments. *J. Asian Earth Sci.*
- Wang, Y., Cheng, H., Edwards, R.L., He, Y., Kong, X., An, Z., Wu, J., Kelly, M.J., Dykoski, C.A., Li, X., 2005. The Holocene Asian monsoon: links to solar changes and North Atlantic climate. *Science* 308, 854–857.
- Wang, Y., Cheng, H., Edwards, R.L., Kong, X., Shao, X., Chen, S., Wu, J., Jiang, X., Wang, X., An, Z., 2008. Millennial-and orbital-scale changes in the East Asian monsoon over the past 224,000 years. *Nature* 451, 1090–1093.
- Wang, Y.-J., Cheng, H., Edwards, R.L., An, Z., Wu, J., Shen, C.-C., Dorale, J.A., 2001. A high-resolution absolute-dated late Pleistocene monsoon record from Hulu Cave, China. *Science* 294, 2345–2348.
- Webster, P.J., Holland, G.J., Curry, J.A., Chang, H.-R., 2005. Changes in tropical cyclone number, duration, and intensity in a warming environment. *Science* 309, 1844–1846.
- West, A.J., Lin, C.W., Lin, T.C., Hilton, R.G., Liu, S.H., Chang, C.T., Lin, K.C., Galy, A., Sparkes, R.B., Hovius, N., 2011. Mobilization and transport of coarse woody debris to the oceans triggered by an extreme tropical storm. *Limnol. Oceanogr.* 56, 77–85.
- Xiao, J., Wu, J., Si, B., Liang, W., Nakamura, T., Liu, B., Inouchi, Y., 2006. Holocene climate changes in the monsoon/arid transition reflected by carbon concentration in Daihai Lake of Inner Mongolia. *The Holocene* 16, 551–560.
- Xue, J., Zhong, W., Cao, J., 2014. Changes in C₃ and C₄ plant abundances reflect climate changes from 41,000 to 10,000 yr ago in Northern Leizhou Peninsula, South China. *Palaeogeogr. Palaeoclimatol. Palaeoecol.* 396, 173–182.
- Yang, T.-N., Lee, T.-Q., Lee, M.-Y., Huh, C.-A., Meyers, P.A., Löwemark, L., Wang, L.-C., Kao, W.-Y., Wei, K.-Y., Chen, R.-F., Chen, H.-F., Chen, S.-H., Wu, J.-T., Shiau, L.-J., Chen, Y.-G., Hsieh, Y.-C., 2014. Paleohydrological changes in Northeastern Taiwan over the past 2 ky inferred from biological proxies in the sediment record of a floodplain lake. *Palaeogeogr. Palaeoclimatol. Palaeoecol.* 410, 401–411.
- Yang, T.-N., Lee, T.-Q., Meyers, P.A., Song, S.-R., Kao, S.-J., Löwemark, L., Chen, R.-F., Chen, H.-F., Wei, K.-Y., Fan, C.-W., Shiau, L.-J., Chiang, H.-W., Chen, Y.-G., Chen, M.-T., 2011. Variations in monsoonal rainfall over the last 21 kyr inferred from sedimentary organic matter in Tung-Yuan Pond, Southern Taiwan. *Quat. Sci. Rev.* 30, 3413–3422.
- Yang, Y., Yuan, D., Cheng, H., Zhang, M., Qin, J., Lin, Y., Zhu, X., Edwards, R.L., 2010. Precise dating of abrupt shifts in the Asian monsoon during the last deglaciation based on stalagmite data from Yamen Cave, Guizhou Province, China. *Sci. China Earth Sci.* 53, 633–641.
- Yuan, D., Cheng, H., Edwards, R.L., Dykoski, C.A., Kelly, M.J., Zhang, M., Qing, J., Lin, Y., Wang, Y., Wu, J., 2004. Timing, duration, and transitions of the last interglacial Asian monsoon. *Science* 304, 575–578.
- Zhang, J., Chen, F., Holmes, J.A., Li, H., Guo, X., Wang, J., Li, S., Lü, Y., Zhao, Y., Qiang, M., 2011. Holocene monsoon climate documented by oxygen and carbon isotopes from lake sediments and peat bogs in China: a review and synthesis. *Quat. Sci. Rev.* 30, 1973–1987.
- Zhang, W., Wu, J., Wang, Y., Wang, Y., Cheng, H., Kong, X., Duan, F., 2014. A detailed East Asian monsoon history surrounding the ‘Mystery Interval’ derived from three Chinese speleothem records. *Quat. Res.*
- Zhao, Y., Yu, Z., Chen, F., Zhang, J., Yang, B., 2009. Vegetation response to Holocene climate change in monsoon-influenced region of China. *Earth Sci. Rev.* 97, 242–256.
- Zheng, F.-L., 2006. Effect of vegetation changes on soil erosion on the loess plateau. *Pedosphere* 16, 420–427.
- Zheng, L.W., Hsiao, S.S.Y., Ding, X.D., Li, D., Chang, Y.P., Kao, S.J., 2015. Isotopic composition and speciation of sedimentary nitrogen and carbon in the Okinawa trough over the past 30 ka. *Paleoceanography* 30, 1233–1244.
- Zhong, W., Cao, J., Xue, J., Ouyang, J., 2015. A 15,400-year record of climate variation from a subalpine lacustrine sedimentary sequence in the Western Nanling Mountains in South China. *Quat. Res.* 84, 246–254.
- Zhong, W., Xue, J., Zheng, Y., Ouyang, J., Ma, Q., Cai, Y., Tang, X., 2010. Climatic changes since the last deglaciation inferred from a lacustrine sedimentary sequence in the Eastern Nanling Mountains, South China. *J. Quat. Sci.* 25, 975–984.
- Zhou, P., Luukkanen, O., Tokola, T., Nieminen, J., 2008. Effect of vegetation cover on soil erosion in a mountainous watershed. *Catena* 75, 319–325.
- Zhou, W., Yu, X., Jull, A.J.T., Burr, G., Xiao, J.Y., Lu, X., Xian, F., 2004. High-resolution evidence from Southern China of an early Holocene optimum and a mid-Holocene dry event during the past 18,000 years. *Quat. Res.* 62, 39–48.